\$ SUPER

Contents lists available at ScienceDirect

#### **Environmental Research**

journal homepage: www.elsevier.com/locate/envres





## High-precision <sup>14</sup>C measurements of parenchyma-rich *Hymenolobium* petraeum tree species confirm bomb-peak atmospheric levels and reveal local fossil-fuel CO<sub>2</sub> emissions in the Central Amazon

Guaciara M. Santos <sup>a,\*</sup>, Rafael Perpétuo Albuquerque <sup>b</sup>, Cláudia Franca Barros <sup>b</sup>, Santiago Ancapichún <sup>c,d</sup>, Rose Oelkers <sup>e</sup>, Laia Andreu-Hayles <sup>e,h,i</sup>, Sergio Miana de Faria <sup>f</sup>, Ricardo De Pol-Holz <sup>c</sup>, Arno Fritz das Neves Brandes <sup>g,\*\*</sup>

- <sup>a</sup> Department of Earth System Science, University of California Irvine, Irvine, CA, 92697-3100, USA
- <sup>b</sup> Instituto de Pesquisas Jardim Botânico do Rio de Janeiro, Escola Nacional de Botânica Tropical, Rio de Janeiro, R.J. 22460-030, Brazil
- <sup>c</sup> Centro de Investigación GAIA Antártica (CIGA), Universidad de Magallanes, Punta Arenas, Chile
- d Postgraduate School in Oceanography, Faculty of Natural and Oceanographic Sciences, Universidad de Concepción, Concepción, Chile
- <sup>e</sup> Lamont-Doherty Earth Observatory of Columbia University, Palisades, NY, USA
- f Centro Nacional de Pesquisa de Agrobiologia, Empresa Brasileira de Pesquisa Agropecuária, Seropédica, RJ, 23890-000, Brazil
- <sup>g</sup> Departamento de Biologia Geral, Instituto de Biologia, Universidade Federal Fluminense, Niterói, RJ, 24210-201, Brazil
- h CREAF, Barcelona, Spain
- i ICREA, Barcelona, Spain

#### ARTICLE INFO

# Keywords: Anthropocene Atmospheric <sup>14</sup>C reconstruction Bomb and post-bomb <sup>14</sup>C periods Parenchyma-rich woods Amazon trees Fossil-fuel emissions

#### ABSTRACT

Atmospheric radiocarbon ( $^{14}$ C) recorded in tree rings has been widely used for atmospheric  $^{14}$ C calibration purposes and climate studies. But atmospheric  $^{14}$ C records have been limited along tropical latitudes. Here we report a sequence from 1938 to 2007 of precisely measured  $^{14}$ C dates in tree rings of the parenchyma-rich *Hymenolobium petraeum* tree species (Porto Trombetas,  $1^{\circ}$ S,  $56^{\circ}$ W) from the Central Brazilian Amazon. *H. petraeum* has discernible growth ring boundaries that allow dating techniques to be employed to produce calendrical dates. Bomb-peak tree-ring  $^{14}$ C reconstruction coincides with the broader changes associated with reported values of the Southern Hemisphere atmospheric  $^{14}$ C curve (SH zone 3; values within the  $\pm 2\sigma$  interval), suggesting that inter-hemispheric air-mass transport of excess- $^{14}$ C injected into the stratosphere during intensive atmospheric nuclear tests is relatively uniform across distinct longitudinal regions. From the early 1980s on-wards, *H. petraeum* had lower  $^{14}$ C values than other pantropical  $^{14}$ C records. Through  $^{14}$ C-based estimation, we found a strong influence of fossil-fuel CO<sub>2</sub> contributions from Porto Trombetas mining operations and shipping traffic on inland waterways. An increase of at least  $6.3 \pm 0.8$  ppm of fossil-fuel CO<sub>2</sub> has been detected by  $^{14}$ C. Our findings invite further  $^{14}$ C analyses using tree rings of tropical tree species as a potential tracer for a wide range of environmental sources of atmospheric  $^{14}$ C-variability.

#### 1. Introduction

Annual tree rings are essential for paleoclimate (Vuille et al., 2012; Morales et al., 2020) and atmospheric radiocarbon (<sup>14</sup>C) reconstructions (Hogg et al., 2020; Reimer et al., 2020; Hua et al., 2021). After thorough cellulose extractions and <sup>14</sup>C measurements, dated tree rings can provide information about atmospheric circulation, ocean-atmosphere CO<sub>2</sub> exchange, and cosmogenic events, among others (Hua et al., 2012;

Rodgers et al., 2011; Brehm et al., 2021). Past atmospheric <sup>14</sup>C reconstructions based on tree-ring measurements are still limited and concentrated at the extratropical regions (Reimer et al., 2020), being almost null along equatorial latitudes.

The convergence of trade winds of both hemispheres occurs along the Equator, creating an asymmetric zone of low atmospheric pressure called the Tropical Low-Pressure Belt (TLPB), also referred to as the intertropical convergence zone (Hua et al., 2021) (Fig. 1). In tropical

<sup>\*</sup> Corresponding author. Department of Earth System Science, University of California, Irvine, Irvine, CA, USA.

<sup>\*\*</sup> Corresponding author. Instituto de Biologia, Universidade Federal Fluminense, Niterói, RJ, Brazil. E-mail addresses: gdossant@uci.edu (G.M. Santos), arnofritz@id.uff.br (A.F. das Neves Brandes).

South America (SA), the December-to-February-TLPB (DJF-TLPB, or SH Zone 3, as defined by Hua et al., 2021) is associated with the summer monsoon, which modulates precipitation and temperature across this region (Vuille et al., 2012). The scarcity of atmospheric 14C records across the TLPB has been associated mostly with the difficulty of finding annual resolved tropical tree-ring archives suitable for atmospheric <sup>14</sup>C reconstructions. While recent studies in dendrochronology have reported an increased number of successful tree-ring chronologies in the tropical regions (Brienen et al., 2016), problems persist in determining tree species' annual ring formation using conventional approaches (e.g., Wils et al., 2009; Herrera-Ramirez et al., 2017; Baker et al., 2017; Haines et al., 2018; Santos et al., 2021). Hence, it is paramount that selected tree species and sites undergoing <sup>14</sup>C reconstructions be properly evaluated by independent robust dating techniques (Andreu-Hayles et al., 2015; Linares et al., 2017; Santos et al., 2020, 2021; Hua et al., 2021). before <sup>14</sup>C time-series can be derived.

Tropical tree species often have parenchyma-rich wood. The main function of parenchyma tissues is to store and mobilize nonstructural carbon (NSC), such as soluble sugars and starches. Early studies on treering <sup>14</sup>C data show the presence of NSCs biasing <sup>14</sup>C signatures, when chemical extractions employed failed to isolate structural cellulose (Cain and Suess, 1976; Worbes and Junk, 1989). A recent work by Slotta et al. (2021) states that slow-turnover NSCs embedded in parenchyma-rich structural cellulose can significantly bias <sup>14</sup>C results, putting into question the use of several woody species found across TLPB for atmospheric <sup>14</sup>C reconstructions.

Here, we investigate the atmospheric <sup>14</sup>C levels recorded by the parenchyma-rich tree species Hymenolobium petraeum (Porto Trombetas; 1°S, 56°W, Fig. 1) in the Central Amazon. While working with Hymenolobium mesoamericanum from Costa Rica, Fichtler et al. (2003) have suggested distinct annual growth rings, and open the possibility of investigating other Hymenolobium tree species. Linares et al. (2017) conducted <sup>14</sup>C analyses using the *H. petraeum* tree shown in this study. Based on <sup>14</sup>C measurements of eight calendar years, spread out between 1950 and 1997, they indicated that this tree species undergoes annual growth. Therefore, we expect that by producing a high-resolution <sup>14</sup>C record for the middle-eastern area of the Amazon Basin based on H. petraeum tree rings, we will be able to i) establish the extent to which our chemical cellulose extractions are capable of producing high-resolution <sup>14</sup>C data of parenchyma-rich tree species; ii) compare the <sup>14</sup>C signatures of dated tree rings of H. petraeum against those of atmospheric calibration curves, which would allow us to assess the reliability of using tropical woods for extending atmospheric <sup>14</sup>C datasets; and finally, iii) add information on environmental dynamics (e.g., TLPB variability and human activities) over tropical SA from the bomb and post-bomb periods.

### 2. Status of bomb and post-bomb atmospheric <sup>14</sup>C datasets across TLPB

The large-scale above-ground thermonuclear bomb tests carried out in the Northern Hemisphere (NH) almost doubled the tropospheric  $\Delta^{14}{\rm C}$ 

level during early 1960s from its natural values. Peak maximums close to 1000‰ in  $\Delta^{14} C$  were observed between 1963 and 1964 in the NH, while an excess of about 670‰ was detected in the Southern Hemisphere (SH) during 1965. Once the Partial Test Ban Treaty of 1963 was signed, tropospheric  $^{14} C$  started decreasing, mainly through air-sea exchange, biosphere uptake, and dilution by  $^{14} CO_2$ -fossil emissions. Large differences in hemisphere peak values were attributed to atmospheric transport within hemisphere mixing cells. Thus, five  $^{14} C$  zones (three in the NH—e.g., NH Zone 1, NH Zone 2, and NH Zone 3—and two in the SH – SH Zone 1–2 and SH Zone 3) have been defined (Hua et al., 2003). Current atmospheric  $^{14} C$  compilations for the zones close to the Equator, i.e., NH Zone 3 and SH Zone 3, are still highly incomplete (Fig. 1), as they are based on shorter datasets and fewer locations.

In a recent global compilation (Hua et al., 2021), the intra-hemispheric NH Zone 3 14C curve indicates the content of two tree-ring datasets (Mandla, India, at 23°N, 81°E [1955-1970] and Doi Inthanon, Thailand, at 18°N, 98°E [1950-1972]) and one atmospheric station (Debre Zeit, Ethiopia, at 8°N, 38°E [1963-1969]). A single dataset from Muna Island, Indonesia (5°S, 122°E [1950-1979]), has been the baseline for the entire atmospheric <sup>14</sup>C intra-hemispheric SH Zone 3 (DJF-TLPB). SH Zone 3 has been delimited to a region comprised between the equatorial line and the SH portion of the entire TLPB area (Fig. 1). Over SA, SH Zone 3 includes most of the Amazon Basin. As yet, no SA dataset at lower latitudes has been produced to reveal east-west <sup>14</sup>C offsets across the TLPB line. On the other hand, a couple of atmospheric <sup>14</sup>C records from the mid-latitudes over SA—Camanducaia, in Brazil (22°50'S, 46°04'W [1950-1997]; Santos et al., 2015), and Irruputuncu, Altiplano, in Chile (20°S, 68°W [1950-2014]; Ancapichún et al., 2021)—have been added to help establish the TLPB boundaries (Fig. 1).

From 1972 onwards, all datasets in the SH have been combined into a single compilation to represent atmospheric <sup>14</sup>C distributions from latitudes ranging from 0 to 90°S. In addition, the global atmospheric <sup>14</sup>C compilation assumes that within each hemisphere tree species growth always falls during the same summer season (e.g., in the NH [June–August] and in the SH [December–February]). While many sites within the TLPB experience little seasonal variation, they can have divergent rainy and dry seasons (Michot et al., 2018), which can directly affect the growing season. Therefore, the current compilations of NH Zone 3 and SH Zone 3 do not contain enough information to define internal controls of <sup>14</sup>C offsets across TLPB, such as different regional atmospheric circulation patterns and/or intra-annual temporal offsets due to growing season distinctions.

#### 3. Structural ring cellulose and nonstructural carbohydrates

NSCs are products of plant photosynthesis. They consist mainly of mobile sugars and immobile starch and lipids. Once NSCs are formed, they are assimilated to produce new tissues, used in metabolic processes, or set aside for future use. Although the functional role of NSC storage and its regulation is not fully understood (Hoch, 2015), the NSCs levels in wood plant are considered an important indicator of plant capacity to

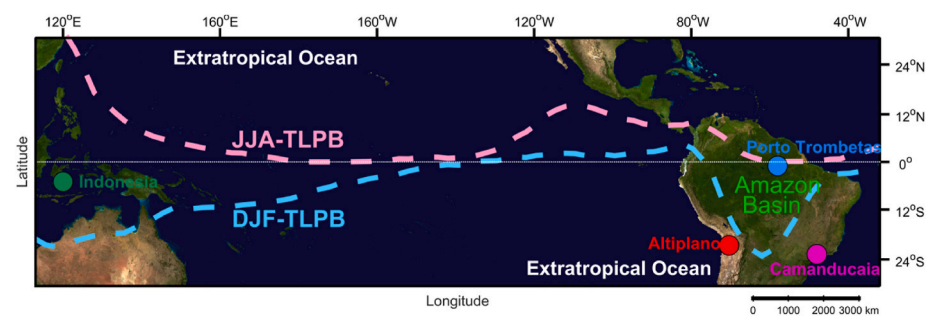


Fig. 1. Locations of  $\Delta^{14}$ C records used in our study: Porto Trombetas (*Hymenolobium petraeum*; 1°S, blue dot; this study); Altiplano (*Polylepis tarapacana*; 20°S, red dot; Ancapichún et al., 2021); Indonesia (*Tectona grandis*; 5°S, green dot; Hua et al., 2012); and Camanducaia (*Araucaria angustifolia*; 22°S; magenta dot; Santos et al., 2015). Shaded pink and light blue lines represent the average latitudinal positions of JJA-TLPB and DJF-TLPB (obtained from Hua et al., 2021), respectively. The Equator is shown with the white dotted line. (For interpretation of the references to color in this figure legend, the reader is referred to the Web version of this article.)

carbon-stress events (Martínez-Vilalta et al., 2016). As for NSC storage amounts in tree stems alone, they are broadly estimated by the percentage of ray and axial parenchyma (Plavcová and Jansen, 2015) and the presence of living fibers (Plavcová et al., 2016). While parenchyma cells can vary considerably among tree species worldwide, they are more abundant in tropical than in temperate trees (Alves and Angyalossy-Alfonso, 2002; Wheeler et al., 2007; Spicer, 2014; Morris and Jansen, 2016; Morris et al., 2016).

Plant parts known to contain slow-remobilized NSCs (or "aged" NSCs) are the shoots and roots (Gaudinski et al., 2009). Richardson et al. (2013, 2015) demonstrated that extractable NSCs contained within stem wood can be older than their structural cellulose counterpart where they are originally stored. However, their findings also suggested that even trees containing aged NSCs would prefer to form structural cellulose from comparatively recent photosynthetic carbon (i.e., <1 year old; Richardson et al., 2015). Therefore, it is important to distinguish between NSCs and structural cellulose chemical processing, plant parts, types of measurements, and results, when comparing different studies and their main goals.

Works stating that stem wood tissue is formed by a mixture of fastand slow-remobilized NSCs were based on isotopic measurements of chemically untreated (Keel et al., 2006; Mildner et al., 2014) or minimally treated wood (acid-base-acid; Trumbore et al., 2015). Even though soluble (sugars) and insoluble (starches) 14C results appear aged in Trumbore et al. (2015), those from minimally treated woods matched with atmospheric 14CO2 records due to effective removal of NSC extracts. For highly resolved post bomb <sup>14</sup>C excursions of precisely dated tree-ring chronologies of pantropical tree species, studies have shown that both alpha-cellulose or holocellulose extractions work well to isolate structural carbon: e.g., Araucaria angustifolia (Santos et al., 2015, Fig. 1), Auracaria araucana (Hadad et al., 2015), and several Cedrela species reported in Baker et al. (2017). In sum, <sup>14</sup>C measurements of specific NSCs (sugars and starches) show the turnaround time of carbon reserves (Carbone et al., 2013), while structural cellulose extracts (alpha-cellulose and/or holocellulose) indicate the time of tissue formation (Santos et al., 2021).

#### 4. Material and methods

#### 4.1. Tree species and site characteristics

Trees of *Hymenolobium petraeum* Ducke (Leguminosae) are big, reaching up to 40 m in height and 1 m in diameter at breast height. They grow in the Amazon forest and have as vernacular names angelim, angelim-pedra, faveira-branca, angelim-escamoso, and angelim-domato (Flora do Brasil 2020, 2021). *H. petraeum* wood is heavily exploited in Brazil (Farani and Oliveira, 2019; Brandes et al., 2020) because of its natural beauty and excellent mechanical properties (Mainieri and Chimelo, 1989).

The wood samples analyzed here are from a single tree of *H. petraeum*, recorded by the number NITw723 in the Wood Collection of the Niterói Herbarium (Xiloteca do Herbário de Niterói). The samples were collected in April 2008 at Porto Trombetas, a district of Oriximiná, Pará State, Brazil (1°27′59″S, 56°22′45″W) (Fig. 1). The climate pattern in the region is the tropical monsoon (Am by Köppen's climate classification) (Alvares et al., 2013) with a dry season. The rainy season runs from December through May (Michot et al., 2018). Yearly rainfall is typically 2260 mm. The annual temperature minimum and maximum are 21.8 °C and 32.7 °C, respectively (Fig. S1).

Axial parenchyma abundance in *H. petraeum* wood stem can constitute a large part of this wood (>25%), with thick bands well supplied with the axial paratracheal confluent parenchyma (Mainieri and Chimelo, 1989; Ferreira and Hopkins, 2004; Botosso, 2009) (Fig. 2A and B). Distinct annual growth rings are delimited by marginal axial parenchyma (Mainieri and Chimelo, 1989; Ferreira and Hopkins, 2004) (Fig. 2B).

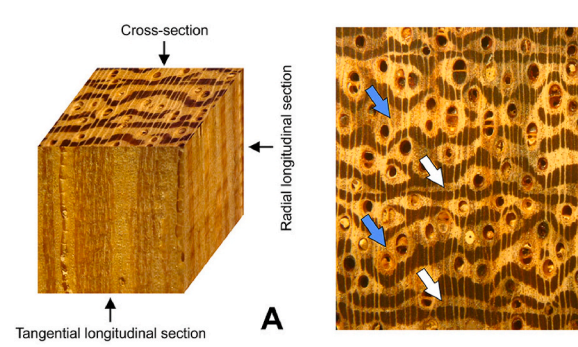


**Fig. 2.** Anatomical views of *H. petraeum* wood through A) 3D wood representation, and B) cross-section view detailing anatomical features – predominance of paratracheal axial confluent parenchyma making bands (blue arrows) and marginal axial parenchyma (white arrows) delimiting tree rings. (For interpretation of the references to color in this figure legend, the reader is referred to the Web version of this article.)

In accordance with other studies (e.g., Hua et al., 2003; Turney et al., 2018), a single tree species may not be regarded as a traditional candidate to be used for dendrochronology dating due to lack of replication (Linares et al., 2017), it qualifies for post-bomb atmospheric  $^{14}$ C reconstructions where data is lacking, if the tree-ring chronology has been found adequate. Here, several actions were taken to ensure that the assigned calendar years of H. petraeum were correct (section 4.2), and a high-quality  $^{14}$ C time series could be derived (section 4.3).

#### 4.2. Tree-ring dating and <sup>14</sup>C wood sampling

In the field, two radii were obtained from a cross (transverse) section of a H. petraeum stem (Figs. S2A and B). Once in the laboratory, the two radii were polished using sandpaper with progressive granulometry (80-1200 grit size) for microscopic observation. Growth-ring boundaries were detected through a stereomicroscope (Olympus SZ11), while images were taken by a photographic camera (Olympus C5050) attached to the same stereomicroscope and by a scanner (HP Scanjet 2400) with 1200 dpi resolution. Preliminary calendar dates were assigned to the rings using dendrochronological techniques, starting from the last growth ring and moving inward to the center of the tree, following the Schulman convention for the SH (Schulman, 1956). For more details refer to figures S3 and S4, and legend of table S1. We measured tree-ring width with CooRecorder v9.4 software and cross-dated the series with CDendro v9.4 software (Cybis Elektronik and Data AB) (Maxwell and Larsson, 2021). We performed running correlations (40-year time windows, 1-year offsets, Pearson correlation) between radii to evaluate the consistencies of growth patterns within the tree (Fig. S5).

For <sup>14</sup>C tree-ring analysis, a strip of wood approximately 1 cm wide was cut from each provisional dated sample (Fig. S2C), followed by an individual sampling of each ring under a stereomicroscope (Fig. S2D). The maximum tissue of each growth ring was attained by precise cuts close to the individual boundaries. Exceptions occur at two sequences of the radii, and their associated <sup>14</sup>C results will be addressed later. Each ring (sample) was further sliced in the radial plane to reduce its dimension (Fig. S2E), conditioned in an Eppendorf vial labeled with the calendar year determined by dendrochronological techniques. Further cuts to produce replicates of "raw" wood were obtained at the Keck Carbon Cycle Accelerator Mass Spectrometer at the University of California Irvine (KCCAMS/UCI) by holding each tree ring in a miniature table vise (TTC 77T 2-1/2" Jaw Width, 3-1/2" Jaw Opening) and using a hand saw (DEWALT 6 in. Jab Saw). While this type of cutting is complex, accurate separation of full tree rings was also attained (Fig. S2F).

#### 4.3. High-precision <sup>14</sup>C measurements

To attain accurate and precise <sup>14</sup>C values, all samples must undergo specific protocols, including reference materials subjected to the same procedures. Subfossil wood (FIRI-H), post-AD 1950 <sup>14</sup>C barley mash (FIRI-J), and <sup>14</sup>C-free wood blank (AVR-07-PAL-37) were chosen for quality control and background corrections of the alpha-cellulose chemical extractions (Santos et al., 2020, 2021), and for subsequent sample processing to filamentous graphite (Santos and Xu, 2017).

Tree rings, as well as reference materials, were chemically processed at two laboratories: the KCCAMS/UCI and the Lamont Doherty Earth Observatory (LDEO). Both laboratories conducted alpha-cellulose extractions using their own procedures. Differences can be summarized as follows: At KCCAMS/UCI, tree rings and reference materials were chemically treated in pre-baked 13 mm culture tubes after samples were carefully reduced to chips and re-weighed. Wood losses during cutting were <3%, even though *H. petraeum* is incredibly dense and difficult to cut. Wood chips were then subjected to cycling 1 N HCl and NaOH at 70 °C until a clear supernatant was reached. To isolate holocellulose, a bleaching step with 1 N HCl-NaClO2 at 70 °C was employed for approximately 6 h. Alpha-cellulose was attained by removing hemicellulose with 17.5% NaOH for 1-2 h at room temperature, followed by 1 N HCl at 70 °C to remove atmospheric CO<sub>2</sub> adsorbed during treatments. Extracts were rinsed by lukewarm ultrapure water to pH neutral, homogenized, and dried for later processing. At LDEO, alpha-cellulose extractions were taken in a 150-funnel custom-made system coupled with a controlled-heated water bath, where chemicals can pass through individual samples (Andreu-Hayles et al., 2019). The chemicals employed are similar to those of KCCAMS/UCI, except for the addition of a carbon-containing buffer (acetic acid, CH<sub>3</sub>CO<sub>2</sub>H) during the bleaching steps. For removal of CH<sub>3</sub>CO<sub>2</sub>H residues from extracted fibers as well as atmospheric CO2 adsorbed during treatments, a 1 N HCl warm bath was added to the original LDEO chemical protocol (details in Santos et al., 2020).

All extracts were further processed to filamentous graphite at KCCAMS/UCI following Santos and Xu (2017) protocols. Radiocarbon measurements were taken on a modified compact AMS system with  $^{13}\text{C}/^{12}\text{C}$  measurement capabilities (NEC 0.5MV1.5SDH-1) to allow for online  $\delta^{13}\text{C}\text{-AMS}$  isotopic-fractionation corrections. By performing all measurements in a single spectrometer, variations in results were limited to inter-laboratory extractions. Accuracy and precision based on reference materials were better than 0.3%. The *H. petraeum*  $^{14}\text{C}$  tree-ring (1938–2007) results, as decay-corrected  $\Delta^{14}\text{C}$  (the deviation from an atmospheric standard and corrected for fractionation; Stuiver and Polach, 1977), are reported in Table S1. In addition, several duplicates and triplicates were rendered using distinct raw wood cuts (Fig. S2).

#### 4.4. Stable isotope analysis

To provide a time series of cellulose  $\delta^{13}C$  values, we measured the remaining homogenized extracts associated with the atmospheric  $^{14}C$  record. Samples were weighed out into  $5\times 9$  mm tin capsules (Costech Analytical Technologies Inc., Valencia, CA, USA) using a microbalance (Sartorius AG, Göttingen, Germany). Total C content and  $\delta^{13}C$  were attained using a Fisons NA-1500NC elemental analyzer (EA) equipped with a Delta-Plus CFIRMS stable-isotope mass spectrometer (IRMS). The  $\delta^{13}C$  results were measured as the ratio of the heavier isotope to the lighter isotope ( $^{13}C/^{12}C$ ), and reported as  $\delta$  values in parts per 1000 or per mil (‰) related to the Vienna Pee Dee Belemnite (VPDB) international standard. Accuracy/precision of 0.01% was attained on recognized EA-IRMS (e.g., USGS24 and atropine,  $C_{17}H_{23}NO_3$ ) and in-house standards.

#### 4.5. Geographical provenance of air parcels to tree-ring site

Hybrid Single-Particle Lagrangian Integrated Trajectory Model

(HYSPLIT v. 4) was used to assess the geographical provenance of the air parcels that potentially transported the <sup>14</sup>CO<sub>2</sub> fixed in the NITw723 tree of Porto Trombetas (Stein et al., 2015). This model supports a wide range of atmospheric transport simulations. The backward trajectories calculated using HYSPLIT are generated as a set of longitudinal, latitudinal, and altitudinal data based on an arbitrary number of hours in the past for a specific hour of the day. Previous studies have shown that 120 h (5 days) is a suitable time window to overcome potential biases, as shorter time windows may show limited trajectories close to the study site, and longer time windows may be associated with major propagation errors (Scarchilli et al., 2011; Schlosser et al., 2008; Sinclair et al., 2013). For tropical SA, Ancapichún et al. (2021) showed that one backward trajectory per day (specifically at midday) is sufficient to represent its general geographical provenance pattern. Thus, 1 daily backward trajectory between January and April, and from 1949 to 2007 (7080 computed trajectories) was chosen. Satellite data and in situ observations of atmospheric variables (the National Centers for Environmental Prediction-National Center for Atmospheric Research products, or just NCEP/NCAR reanalysis) were used as the input data of the HYSPLIT model (Kalnay et al., 1996).

#### 4.6. Concentration of fossil-fuel CO2

Fossil-fuel concentrations (ppm) were estimated using the equation presented in Levin et al. (2003):

$$CO_2 Fossil = CO_2 local \frac{\Delta^{14} C_{bg} - \Delta^{14} C_{local}}{\Delta^{14} C_{bg} + 1000}$$
 (1)

where  $CO_2$  fossil is the estimated mole fraction (ppm) of  $CO_2$  derived from fossil emission sources.  $CO_2$  local is the atmospheric  $CO_2$  mole fraction in the local region (the Equator,  $0^\circ$ ) and was obtained from Earth System Research Laboratories (Dlugokencky and Tans, 2020);  $\Delta^{14}C_{local}$  and  $\Delta^{14}C_{bg}$  are the  $\Delta^{14}C$  for local (i.e., Porto Trombetas with the value associated with 1984 obtained through linear interpolation) and background regions, respectively. We used two potential background series: SH Zone 3 (Hua et al., 2013) and Camanducaia (Santos et al., 2015). The SH Zone 3 series (1950–2010) represents atmospheric  $^{14}C$  concentrations without Amazon influence. The Camanducaia series (1928–1998) represents atmospheric  $^{14}C$  concentrations with Amazon influence. Uncertainties were calculated using the Monte Carlo method.

#### 5. Results and discussion

#### 5.1. Dating of H. petraeum and carbon isotopic analysis

The two radii of the same tree were successfully cross-dated. The correlation coefficient between the two tree-ring width time series was 0.44 (T-test: 7.0), overlapping 203 years (1805–2007; Schulman years). The running correlation, using a 40-year time window lagged 1 year, showed the highest correlation (>0.50) from 1888 to 1927 to 1943–1982 (Fig. S5). Under traditional tree-ring analysis, sampling many trees and cross-dating radii within the same tree and among trees is paramount (Fritts, 1976; Speer, 2010; Hughes et al., 2011). However, a special exception is given for tree species and sites where <sup>14</sup>C data is nonexistent or extremely scarce (Hua et al., 2003, 2021; Turney et al., 2018). Further criteria were then adopted for enhancing this <sup>14</sup>C time series.

The *H. petraeum* tree of Porto Trombetas presents well-defined annual tree rings that are cross-datable between both radii (Fig. S5). However, the generation of this tree-ring record to produce a fine-tuned atmospheric <sup>14</sup>C reconstruction was challenging due to the presence of growth ring anomalies (Figs. S3 and S4). After the generation of high-precision <sup>14</sup>C-AMS annual measurements using the first radius, some anomalies were detected in the calendar years assigned. On corresponding radii, the tree-ring boundaries were reexamined by finer

anatomical analysis, and the 1968, 2001, and 2007 calendar dates were confirmed to be misidentified. Wedging rings, faint growth ring boundaries, and narrow growth rings appear to be the causes of those growth ring misidentifications (Figs. S3 and S4). The abundant confluent parenchyma and marginal parenchyma, especially in narrow rings, complicated the detection of growth ring boundaries and sampling of wood material. However, the high number of overlapping tree rings/<sup>14</sup>C measured in this study (72 from radius 1, and 50 from radius 2) and careful anatomical analyses, ensure that atmospheric  $^{14}\mathrm{C}$  signatures were accurately determined for this site. Both analyses allowed us to properly resolve the dating ambiguities found in the preliminary dated tree-ring series of NITw723, so that calendar dates in this study do not appear resolved by <sup>14</sup>C results alone. Replication of random calendar dates, including distinctive chemical extractions in two laboratories (56 from KCCAMS/UCI and 66 from LDEO), ensured high reproducibility of results. A pooled standard deviation calculation determined that replicated measurements are within the 0.3% level or better (n = 27 pairs/ sets), with the exception of 1962 (quadruplicates yielded 0.9%). Tree rings from 1942, 1966, 1968, 2001 to 2003, and 2007 were not sampled or measured by <sup>14</sup>C (e.g., narrow or wedged ring; Table S1). A total of 122 <sup>14</sup>C-AMS results were produced from the two radii with overlapping uncertainties (Table S1).

The *H. petraeum* <sup>14</sup>C signatures matched the expected atmospheric levels across TLPB, as shown in Fig. 3A. The averaged <sup>14</sup>C-AMS data of consecutive single tree rings was compared with both SH atmospheric <sup>14</sup>C compilations (SH Zones 1–2 & 3; as reported in Hua et al., 2013, 2021). Previous studies (Baker et al., 2017; Granato-Souza et al., 2018, 2020) have demonstrated the importance of minimum and maximum precipitation for the onset and duration of wood tissue growth of distinct tree species in the tropics. Thus, we compared the Amazon Basin precipitation information of Porto Trombetas (Fig. S1) with that of Michot et al. (2018), and identified early March for the middle of tissue growth, where precipitation averages are above 250 mm (Fig. S1). Since peak tissue growth was not based on correlation analyses among several trees (e.g., Granato-Souza et al., 2018), an error bar of  $\pm$ 0.3 (covering 6 months) was added to calendar dates to cover precipitation timing and full stem tissue growth (Dec–May).

Excellent agreement between measured <sup>14</sup>C tree-ring data and current SH compilations was found (Fig. 3A), except for the years 1957 and 1958 (shaded area I), in which the separation of tree rings was complicated by very thin bands (Fig. S2; Table S1). No *H. petraeum* <sup>14</sup>C tree-ring data differ significantly from bomb peak values in SH Zone 3,

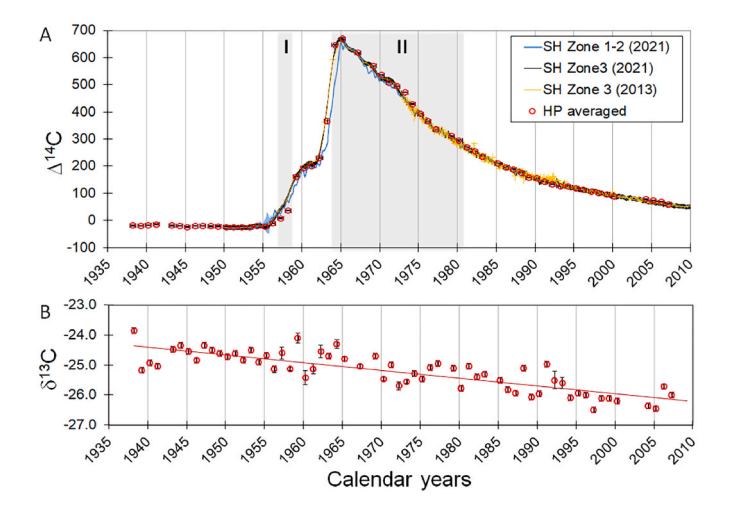


Fig. 3. Averaged  $\Delta^{14}C$  (A) and  $\delta^{13}C$  (B) values running from 1938 to 2007 of a single individual of H. petraeum from Central Equatorial Amazon (1°S, 56°W). Calendar years AD points were adjusted to middle Dec–May (peak of wet season) followed by a six-month uncertainty. Shaded areas correspond to the calendar date sequences 1957–1958 and 1964–1980, respectively.

especially between 1964 and 1980 (shaded area II). This finding is in disagreement to that of Slotta et al. (2021), where a 14C mismatch of 8.8% between cellulose extracts of tree rings of Adansonia digitata (African baobab) from southern Oman (17°N, 54°E) and those of the June-to-August-TLPB bomb-peak atmospheric <sup>14</sup>C curve (JJA-TLPB, NH Zone 3, Hua et al., 2021) was detected. For A. digitata, lower than expected <sup>14</sup>C values were observed from the rising of the bomb peak to the beginning of its decline (ca. 1955–1975; Slotta et al., 2021), leading the authors to assume that the structural cellulose fraction isolated for <sup>14</sup>C analysis contained aged NSCs. For H. petraeum tree species, slow-remobilized NSCs in the structural cellulose fraction (in association with parenchyma-rich tissue; Fig. 2) appear to be irrelevant. Moreover, a key difference between this work and Slotta et al. (2021) is related to the fraction of wood used for isotopic analyses. In our setting, whole rings were sampled, chopped, and chemically extracted to alpha-cellulose as a whole, even when rings (as raw wood) were reduced in size to produce duplicates (Figs. S2E and F). Isotopic measurements to attain  $\Delta^{14}$ C and δ<sup>13</sup>C values were conducted from homogenized alpha-cellulose fibers after chemical extractions reached completion. In Slotta et al. (2021), tree rings (as raw wood) were cut into slices at the terminal parenchyma and intra-annual tangential parenchyma bands, so that rays and other parenchymatous structures could be removed. Later on, 2/3 of each tree ring was used for extractions and 14C-AMS analysis, while 1/3 was reserved for stable isotope measurements. Broadly speaking, it is possible that the cutting strategy deployed to remove parenchymatous structures, in lieu of chemically treating each ring as a whole, led to the loss of recent photosynthesized carbon. In post-bomb <sup>14</sup>C dating, and especially regarding the calendar years surrounding the bomb peak (where dramatic changes in <sup>14</sup>C occur), loss of wood cells from the current growth season would trigger unexpected 14C offsets. Atmospheric <sup>14</sup>C compilations employing tree rings favor whole rings, or pre-selected early- and latewood fractions, all of which must cover a well-defined time frame for accurate atmospheric <sup>14</sup>C determinations (Hua et al., 2021).

Regarding the time series of  $\delta^{13}$ C-IRMS values of alpha-cellulose extracts (Fig. 3B), a linear regression gave a dilution rate of -0.026% year  $^{-1}$ . This is compatible with the global atmospheric (and tree-ring)  $\delta^{13}$ C-decline rate due to CO<sub>2</sub> production from fossil fuel emissions (Tans, 2022). Even though vegetation  $\delta^{13}$ C-IRMS signatures tend to be noisier due to isotopic fractionation effects (Wang and Pataki, 2010), the Central Amazon  $\delta^{13}$ C-series showed the same Great Acceleration (industrialization and economic growth) observed by others (Turney et al., 2018), which can be attributed to fossil emissions outflowing from the NH (Suess effect).

#### 5.2. Bomb and post-bomb <sup>14</sup>C values in the Central Amazon

To point out patterns in our H. petraeum <sup>14</sup>C dataset, in Fig. 4A we display the  $\Delta^{14}$ C difference between our results and those for the SH Zone 3 compilation of Hua et al. (2021). Most sizeable differences arose during the 1960–1965 period, where aboveground nuclear explosions of multiple intensities occurred (Enting, 1982), inducing a heterogeneous large increase of <sup>14</sup>C in the Earth's atmosphere. The remaining computed H. petraeum <sup>14</sup>C values are not significantly different from Hua et al. (2021) compilation.

While we expected a reasonable match between records from the same latitudinal zone, we also expected to observe continuous and increased <sup>14</sup>C values after the bomb peak for a record at the core of the Amazon Basin, such as *H. petraeum* (1°S, 56°W), due to biosphere-to-atmosphere CO<sub>2</sub> exchange flux. This assessment aligns with an early model by Randerson et al. (2002) regarding the geographical differences of the atmospheric excess-<sup>14</sup>C through tropical lands, which forecasted a persistent <sup>14</sup>C increase after mid-1980. This counterintuitive hypothesis was first detected in a middle-latitude <sup>14</sup>C record, from Camanducaia (Santos et al., 2015), due to its location (Fig. 1) and distinct air masses influencing <sup>14</sup>C signatures (discussed below). For these reasons, the

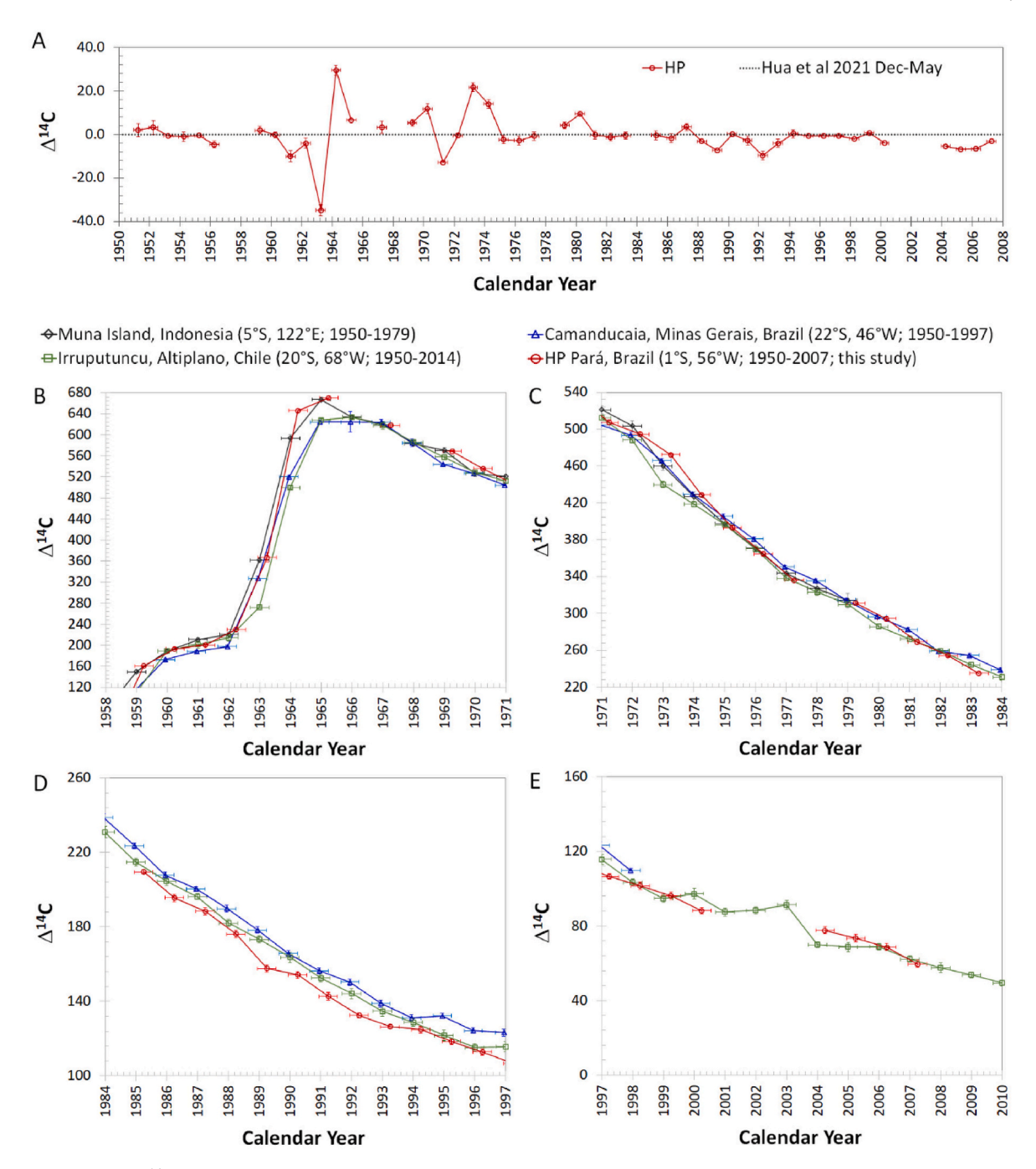


Fig. 4. Panel (A) monthly  $\Delta^{14}$ C differences between the *H. petraeum* (HP) tree-ring record and the SH Zone 3 compilation of Hua et al. (2021). Here, only the atmospheric <sup>14</sup>C signals spread between December and May in the SH Zone 3 profile have been used. Panels (B to E) show direct comparisons of the *H. petraeum*  $\Delta^{14}$ C record versus standalone pantropic datasets. Data points associated with calendar years (AD) were plotted according to the growth period information provided on publications, and overall, they cluster around the end or beginning of each year (depicting the austral summer). A  $\pm 0.3$  yrs error was added to cover total stem tissue growth. Each panel shows 13 calendar years, starting from 1959 onward. For continuity purposes, calendar years overlap in these multi-panel plots.  $\Delta^{14}$ C error bars are  $\pm 1\sigma$ . Standalone dataset ranges are displayed in the figure labels.

almost exact match between the *H. petraeum* record and the SH Zone 3 compilation from 1974 and beyond is somewhat unexpected (Fig. 4A), as the late segment of the Hua et al. (2021) compilation was determined mostly by high-latitude SH  $^{14}\mathrm{C}$  records. Moreover, the *H. petraeum*  $^{14}\mathrm{C}$  record becomes even lower during the late 1980s and early 1990s, as well as during the middle 2000s, suggesting that other factors may be in play.

To better understand the occurrence of differences between records, we broke down the bomb-peak into 4 plots (Fig. 4B, C, D, and E) and compared our record to standalone tree ring datasets in the tropics.

Fig. 4B shows how well the *H. petraeum* record aligned with *Tectona grandis* (Indonesia) for the bomb-peak period. Here, the atmospheric mass transfer between the NH and SH appears to be fairly consistent, and independent of the large longitudinal difference between these sites (Fig. 1). Roughly,  $\Delta^{14}$ C values derived from these two records are analogous (Table S2), even though *H. petraeum* tissue growth peaks a couple of months after that of *T. grandis* tree species (i.e., early March rather than early January). A large difference (52.7  $\pm$  7.1‰) is noted with the 1964 calendar year between *H. petraeum* and *T. grandis* records (Table S2), with the former  $\Delta^{14}$ C value the highest. Since wood recovery

during sample processing is rather important, and our H. petraeum 1964 <sup>14</sup>C value (Fig. 5B and Table S2) is an average of four measurements of wood cuts sampled from the two radii, we suspect that the  $\Delta^{14}$ C difference observed here may be attributed to T. grandis partial wood loss during processing. Without further high-precision <sup>14</sup>C results from this latitudinal zone, other explanations for the difference would be futile. On the other hand, we attained an excellent agreement for the bomb peak calendar year of 1965 (i.e., a difference of 3.2  $\pm$  5.5%) and subsequent calendar years (even though we are missing 1966 and 1968; Table S2). Our results, in the allotted timeframe shown in Fig. 4B, support that inter-hemispheric air-mass transport of excess-14C injected in the stratosphere during intensive atmospheric nuclear tests appears to be uniform across distinct longitudinal regions: i.e., Indonesia and Central Amazon, Moreover, these results also reinforced the lack of aged NSCs in the structural cellulose extracts, as addressed earlier. In terms of the tree-ring <sup>14</sup>C records at middle latitudes—i.e., SH Zones 1–2—data from Altiplano and Camanducaia also correlate relatively well with each other during this period (Fig. 4B).

In the early 1970s, H. petraeum <sup>14</sup>C values were overall higher than other pantropical SH records (Fig. 4C), corroborating the post-bomb biocarbon recycling hypothesis of Randerson et al. (2002) model, as expected for a site at 1°S within the DJF-TLPB airflow. Enriched <sup>14</sup>CO<sub>2</sub> contributions from deforestation and vegetation fires seemed an unlikely explanation for these high  $\Delta^{14}$ C values, as they normally occur in the Basin during the dry season (Jun-Nov; Fig. S1). The first known example of <sup>14</sup>C enrichment due to post-bomb bio-carbon recycling belongs to the SA tree-ring record of Camanducaia (22°S, 46°W). Even though this record and Altiplano (20°S, 68°W) are within the same latitudinal range (north of the Tropic of Capricorn, and at each side of the TLPB potential boundaries over this continent; Fig. 1), only Camanducaia shows <sup>14</sup>C continuous enrichment from the 1970s onward. The persistent increased <sup>14</sup>C values of the Camanducaia record have been attributed to air parcels from geographical provenances at the SH Atlantic extratropical ocean and the Amazon Basin. Through air-parcel modeling, Ancapichún et al. (2021) projected that a high <sup>14</sup>C level flux (relative to other SH geographical locations) from the Amazon biosphere during the post-bomb period can reach adjacent zones at the edge of the TLPB boundary, and thereby increase their atmospheric  $\Delta^{14} C$  values. However,  $\Delta^{14} C$  values from our Central Amazon H. petraeum record moved toward other pantropical SH records during the middle 1970s, followed by a sudden decrease in  $\Delta^{14}$ C values just before 1983 (Fig. 4D).

Basically, from the 1980s onward  $\Delta^{14}C$  values from our Central Amazon record remain lower than all other pantropical SH records, including the  $\Delta^{14}C$  values that were computed in the SH Zones 1–2 and 3 compilations (Fig. 4A). From the middle 1990s,  $^{14}C$  values reverse to slightly higher values than in the early decade (Fig. 4C and D). However, those values are still too low to reflect airflow carbon signatures, which are mostly dominated by transatlantic regions during the DJF-TLPB, and/or the eastern Amazon geographical provenances (Fig. 5).

Since a significant number of <sup>14</sup>C replicates have been produced for the H. petraeum record (Table S1), sample and measurement problems cannot be invoked. Whereas Slotta et al. (2021) suggested the possibility of aged NSCs in structural cellulose of parenchyma-rich woods as a source of <sup>14</sup>C bias, we have not observed this effect here. H. petraeum highest portion of the bomb-peak profile matched with expected values (Fig. 3A). Thus, from 1980s onward <sup>14</sup>C-depletions at the *H. petraeum* record (Fig. 4B–C) must be due to close proximity to <sup>14</sup>C-free fossil fuel CO2 sources. Since active volcanoes and/or usage of coal for cooking (rather than fuelwood) are unlikely in this region, we are left with petroleum-based byproducts (i.e., gasoline, diesel and crude oil) as possible sources. These types of fuels are wildly use in power generation and transportation. The low population density (0.5/km<sup>2</sup>) of the rural community of Oriximiná cannot be tied to the bulk-production of <sup>14</sup>C-free fossil fuel CO<sub>2</sub> emissions responsible for the <sup>14</sup>C depletions detected here.

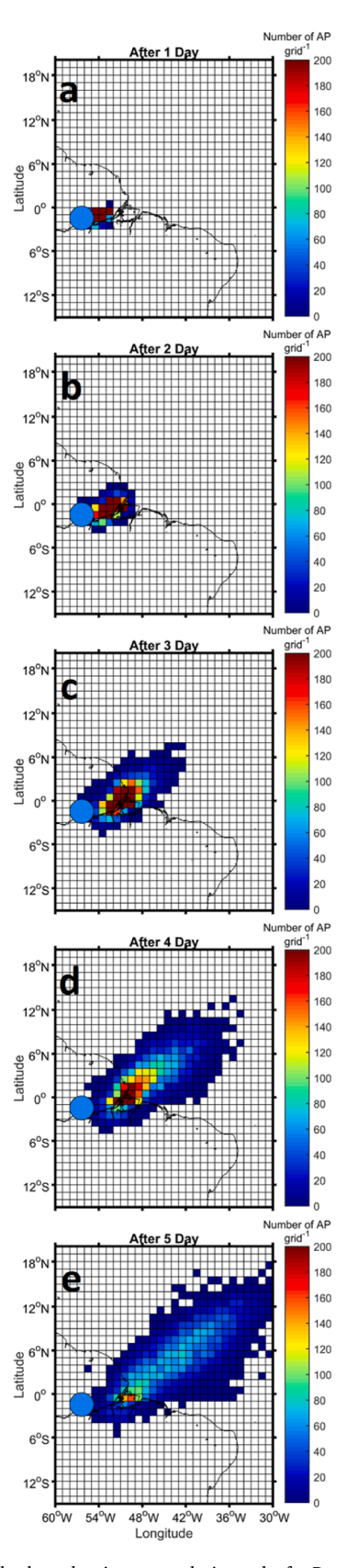


**Fig. 5.** HYSPLIT backward trajectory analysis results for Porto Trombetas (1 h per day, midday). Air parcel density arriving at our site. The color bar scale indicates the total number of air parcels located on each pixel grid ( $1^{\circ} \times 1^{\circ}$ ) at hour: -24 (a), -48 (b), -72 (c), -96 (d), and -120 (e) during the bomb period (January to April 1949 to 2007). (For interpretation of the references to color in this figure legend, the reader is referred to the Web version of this article.)

The level of decreases in  $\Delta^{14}$ C values observed in the *H. petraeum* record coincides in time with the implementation of large-scale industrial bauxite ore mining operations (the raw material used to produce aluminum) and shipping activities at Porto Trombetas (Fig. S6). The Trombetas Bauxite Mine was established in 1976 with a complete mineral processing infrastructure, and multimodal transportation hub (Bebbington et al., 2018). Porto Trombetas is Brazil's largest producer and exporter of bauxite (approximately 70%; Andrade, 2011). Ore mining at this location have been inducing deforestation (Sonter et al., 2017), degradation of lakes (Lin and Caramaschi, 2005) and soils (Guimarães et al., 2018). Since the early 1980s, massive inland waterway transportation has carried products from the Trombetas River into the Amazon River, and later to the sea. Da Cunha et al. (2021) gave a total estimate of over 1000 vessels/year operating in Amazonian waters, with more than 12% designated to Porto Trombetas alone. Moreover, 66% of the total vessels mentioned above are bulk carriers that even when are not in transit (i.e., collecting or offloading cargo at the port) they are still producing air pollution from engine exhaust. Thus, CO<sub>2</sub> pollution by combustion-ignition motors and vessels in association to mining operations in close proximity to the Amazon River and its tributaries are the only likely source for <sup>14</sup>C depletions detected at the H. petraeum record beyond 1980s.

From the middle of the 1990s onward, we detected a small increase of <sup>14</sup>C-values in the Central Amazon record toward SA records (Fig. 4E). A reduction in operations due to a shortage in investments during this period (Mason, 1997), followed by the ongoing reforestation of former mining sites (Parrotta and Knowles, 2001; Bustamante et al., 2019; Gomes et al., 2019) may partially explain the improvement of <sup>14</sup>C-values in the *H. petraeum* record observed here.

Worldwide increases in atmospheric CO2 during the twentieth century are directly related to global economic growth and the dependence of fossil fuel burning (Chiquetto et al., 2022), which can be directly detected by <sup>14</sup>C measurements of air-CO<sub>2</sub> and/or biomass. Studies using <sup>14</sup>C to trace local fossil fuel CO<sub>2</sub> emissions are normally carried on close to known sources: e.g., volcanic vents (Evans et al., 2010) and/or urban infrastructures (Quarta et al., 2007; Vásquez et al., 2022; Chiquetto et al., 2022). Therefore, the evidence presented above strongly suggests a local source of fossil fuel burning. Our  $\delta^{13}$ C values appear to play little to no role in determining this source, possibly due to data noise (Wang and Pataki, 2010). While the Porto Trombetas mining operations are potentially responsible for the dilution of atmospheric <sup>14</sup>CO<sub>2</sub> locally, air parcels reaching our site during the growing season follow the Amazon River path (Fig. 5). Those air masses cover most of the Amazon River mouth, where ship traffic from recent decades is extremely high (Da Cunha et al., 2021). Thus, the Amazon and Trombetas Rivers can be considered a source-area of fossil fuel atmospheric CO2.

To estimate fossil fuel  $CO_2$  excess contributions to the local atmosphere near Porto Trombetas inprint in the H. petraeum  $^{14}C$  record, we used Equation (1) and weight mean and standard error calculations. We determined averaged fossil fuel  $CO_2$  excesses on the order of  $1.4 \pm 0.4$  (based on SH Zone 3 compilation) and  $3.7 \pm 0.3$  ppm (based on Camanducaia  $^{14}C$  record) from 1979 to 1998 (Fig. 6). While those averaged fossil fuel  $CO_2$  levels are still relatively low compared to megacities elsewhere (Chiquetto et al., 2022. and references therein), maximum fossil fuel  $CO_2$  excess of  $6.30 \pm 0.8$  ppm was registered for the calendar year of 1989 using Camanducaia  $^{14}C$  record as background; Fig. 6. Thus, our study evidenced local anthropogenic atmospheric  $CO_2$  changes through burning of fossil fuel due to mega-mining operations and the usage of the Trombetas and Amazon Rivers as open waterways to transport ore as well as other commodities to the Atlantic Ocean (Fig. S6).

Since bauxite ore production at Porto Trombetas has jumped from 2 to 12 million tons/year in just 4 decades (source MRN - https://www.mr n.com.br/), our findings call for urgent action to address atmospheric  $CO_2$  fossil fuel related increases. While mines are adopting sustainable activities to minimize their environmental impacts (Bustamante et al.,

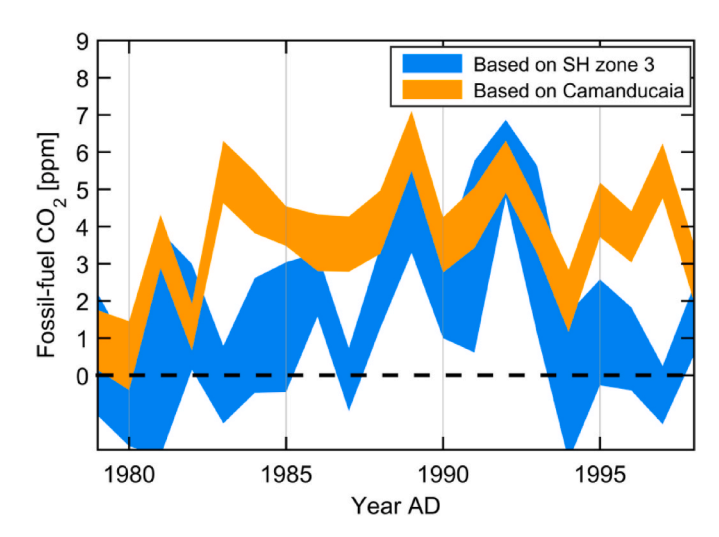


**Fig. 6.** The excess concentration of fossil fuel  $CO_2$  values over time in ppm for the Porto Trombetas between 1979 and 1998. We used two background  $^{14}C$  series: SH Zone 3 (blue, without Amazon influence; Hua et al., 2013) and Camanducaia (orange, with Amazon influence). (For interpretation of the references to color in this figure legend, the reader is referred to the Web version of this article.)

2019), they still rely on external technology changes. Decarbonization of mining operations and ocean freight are difficult, as fossil fuels continue to dominate these sectors. A 5% reduction could be attained by using biofuels and/or blended fuels, but their use in those sectors have been limited. This discussion is out of scope here, but further considerations on how to reach low-carbon emissions in those sectors can be found in Igogo et al. (2021) and Xing et al. (2021).

#### 6. Conclusions

To improve <sup>14</sup>C calibration curves and our understanding of the past variability of global climatic mechanisms, the development of reliable annual atmospheric <sup>14</sup>C reconstructions along tropical latitudes is fundamental. The parenchyma-rich tree species *H. petraeum* collected at the Central Amazon Basin successfully recorded annual atmospheric <sup>14</sup>C levels from 1938 to 2007. The *H. petraeum* atmospheric <sup>14</sup>C signals surrounding the bomb peak (1950–1971) are like those of Indonesia, which is at almost the same latitude in the SH. The fact that these two tree-ring <sup>14</sup>C records relate to one another indicates that bomb-enriched <sup>14</sup>C air masses from NH (once mixed in the equatorial troposphere) were distributed uniformly to our SH site by the latitudinal displacement of the DJF-TLPB.

After 1980, *H. petraeum* atmospheric <sup>14</sup>C signals reveal local fossil-fuel-related emissions from Porto Trombetas as well as those from shipping activities in the Amazon River downstream and estuary areas. Thus, atmospheric  $\Delta^{14}$ C variability in the Central Amazon has a wide range of natural and anthropogenic sources.

Careful sampling and cutting of whole rings, as well as proper chemical procedures to isolate cellulose, allowed us to attain accurate and precise  $^{14}\mathrm{C}\text{-AMS}$  results around the bomb peak. Based on this result, several parenchyma-rich tree species of tropical forests can be evaluated for their growth and quality, as atmospheric  $^{14}\mathrm{C}$  proxies. In this sense, other datasets should be developed from the Amazon Basin, in order to better understand lower-elevation atmospheric  $^{14}\mathrm{C}$  distributions, intraannual differences, post-bomb carbon isoflux responses, carbon residence time in the Amazon biosphere, and local  $^{14}\mathrm{CO}_2$  fossil emissions, among others.

#### CRediT authorship contribution statement

Guaciara M. Santos: Conceptualization, Project administration,

Funding acquisition, Radiocarbon Methodology, Supervision, Investigation, Formal analysis and interpretation, Writing-original draft, Writing-review & editing, visualization, data curation, validation, literature synthesis, and discussion. Arno Fritz das Neves Brandes: Tree-ring Methodology, Supervision, Investigation, Writing-original draft, visualization, data curation, validation, literature synthesis and discussion. Rafael Perpétuo Albuquerque & Cláudia Franca Barros: Tree-ring Methodology and Investigation, Writing—review & editing. Santiago Ancapichun: Formal analysis and interpretation, Writing-original draft, visualization, validation, literature synthesis and discussion. Rose Oelkers: Cellulose extraction methodology, Writing-review & editing.Laia Andreu-Hayles: Cellulose extraction methodology, Funding acquisition, Writing-review & editing. Sergio Miana de Faria: Sample collection, Writing—review & editing. Ricardo De Pol-Holz: Writing —review & editing, literature synthesis and discussion.

#### Data availability

Data pertaining to this research appears in the Supplementary Materials file.

#### Declaration of competing interest

The authors declare that they have no known competing financial interests or personal relationships that could have appeared to influence the work reported in this paper.

#### Acknowledgements

This research was supported by the United States National Science Foundation (AGS-1903690 to G.M.S and AGS-1903687 to L.A-H). G.M.S thanks Anita S. Yayi Komatsu and Jazmine M. Jr. Renteria from UCI for assistance on laboratory procedures. S.A. was supported by PROYECTO CONICYT-BMBF 180005: AVOID. S.M.F. was supported by the National Research Council (CNPq- 561905/2010-0). R.DP-H. was supported by Fondecyt grant 1201810. We also send our appreciation to Daniela Granato-Souza for comments and suggestions in an early version of our manuscript. We sincerely thank the anonymous reviewers and editor.

#### Appendix A. Supplementary data

Supplementary data to this article can be found online at https://doi.org/10.1016/j.envres.2022.113994.

#### References

- Alvares, C.A., Stape, J.L., Sentelhas, P.C., et al., 2013. Köppen's climate classification map for Brazil. Meteorol. Z. 22, 711–728. https://doi.org/10.1127/0941-2948/ 2013/0507.
- Alves, E.S., Angyalossy-Alfonso, V., 2002. Ecological trends in the wood anatomy of some Brazilian species. 2. Axial parenchyma, rays and fibres. IAWA J. 23, 391–418. https://doi.org/10.1163/22941932-90000311.
- Ancapichún, S., De Pol-Holz, R., Christie, D.A., Santos, G.M., Collado-Fabbri, S., Garreaud, R., Lambert, F., Orfanoz-Cheuquelaf, A., Rojas, M., Southon, J., Turnbull, J.C., 2021. Radiocarbon bomb-peak signal in tree-rings from the tropical Andes register low latitude atmospheric dynamics in the Southern Hemisphere. Sci. Total Environ. 774, 145126 https://doi.org/10.1016/j.scitotenv.2021.145126.
- Andrade, L., 2011. Quilombola Lands in Oriximiná: Pressure and Threats. Pro-Indian Commission of São Paulo, 44pages.
- Andreu-Hayles, L., Levesque, M., Martin-Benito, D., Huang, W., Harris, R., Oelkers, R., Leland, C., Martin-Fernández, J., Anchukaitis, K.J., Hellen, G., 2019. A high yield cellulose extraction system for small whole wood samples and dual measurement of carbon and oxygen stable isotopes. Chem. Geol. 504, 53–65.
- Andreu-Hayles, L., Santos, G.M., Herrera-Ramírez, D.A., Martin-Fernández, J., Ruiz-Carrascal, D., Boza-Espinoza, T.E., Fuentes, A.F., MJ, P., 2015. Matching dendrochronological dates with the Southern Hemisphere 14C bomb curve to confirm annual tree rings in Pseudolmedia rigida from Bolivia. Radiocarbon 57 (1), 1–3. https://doi.org/10.2458/azu\_rc.57.18192.
- Baker, J.C.A., Santos, G.M., Gloor, M., Brienen, R.J.W., 2017. Does Cedrela always form annual rings? Testing ring periodicity across South America using radiocarbon dating. Trees. https://doi.org/10.1007/s00468-017-1604-9.

- Bebbington, D.H., Verdun, R., Gamboa, C., Bebbington, A.J., 2018. Impacts of Extractive Industry and Infrastructure on Forests. Assessment and Scoping of Extractive Industries and Infrastructure in Relation to Deforestation. Amazonia.
- Botosso, P.C., 2009. Identificação Macroscópica de Madeiras: Guia Prático e Noções Básicas Para o Seu Reconhecimento. Embrapa Florestas-Documentos (INFOTECA-E). http://www.infoteca.cnptia.embrapa.br/infoteca/handle/doc/736957.
- Brandes, A.F.N., Novello, B.Q., Domingues, G.A.F., et al., 2020. Endangered species account for 10% of Brazil's documented timber trade. J. Nat. Conserv. 55, 125821 https://doi.org/10.1016/j.jnc.2020.125821.
- Brehm, N., Bayliss, A., Christl, M., Synal, H.-A., Adolphi, F., Beer, J., et al., 2021. Elevenyear solar cycles over the last millennium revealed by radiocarbon in tree rings. Nat. Geosci. 14 (1), 10–15. https://doi.org/10.1038/s41561-020-00674-0.
- Brienen, R.J., Schöngart, J., Zuidema, P.A., 2016. Tree rings in the tropics: insights into the ecology and climate sensitivity of tropical trees. Trop. Tree Physiol. 439–461.
- Bustamante, M.M.C., Silva, J.S., Scariot, A., et al., 2019. Ecological restoration as a strategy for mitigating and adapting to climate change: lessons and challenges from Brazil. Mitig. Adapt. Strat. Glob. Change 24, 1249–1270. https://doi.org/10.1007/s11027-018-9837-5.
- Cain, W.F., Suess, H.E., 1976 Jul 20. Carbon 14 in tree rings. J. Geophys. Res. 81 (21), 3688–3694.
- Carbone, M.S., Czimczik, C.I., Keenan, T.F., Murakami, P.F., Pederson, N., Schaberg, P. G., Xu, X., Richardson, A.D., 2013. Age, allocation and availability of nonstructural carbon in mature red maple trees. New Phytol. 200 (4), 1145–1155. https://doi.org/10.1111/nph.12448.
- Chiquetto, J.B., Leichsenring, A.R., dos Santos, G.M., 2022. Socioeconomic conditions and fossil fuel CO2 in the metropolitan area of Rio de Janeiro. Urban Clim. 43, 101176.
- Da Cunha, A.C., De Abreu, C.H.M., Crizanto, J.L.P., Cunha, H.F.A., Brito, A.U., Pereira, N.N., 2021. Modeling pollutant dispersion scenarios in high vessel-traffic areas of the Lower Amazon River. Mar. Pollut. Bull. 168, 112404.
- Dlugokencky, E., Tans, P., 2020. Trends in Atmospheric Carbon Dioxide. National Oceanic and Atmospheric Administration. Earth System Research Laboratory (NOAA/ESRL), available at: http://www.esrl.noaa.gov/gmd/ccgg/trends/global.html. (Accessed 16 October 2020). last access:
- Enting, I., 1982. Nuclear Weapons Data for Use in Carbon Cycle Modeling. CSIRO Division of atmospheric physics and technology, Melbourne (Australia).
- Evans, W.C., Bergfeld, D., McGeehin, J.P., King, J.C., Heasler, H., 2010. Tree-ring 14C links seismic swarm to CO2 spike at Yellowstone, USA. Geology 38 (12), 1075–1078.
- Farani, T.L., Oliveira, G.B., 2019. Produção madeireira de espécie nativas brasileiras (2012 a 2017). Ibama. Brasília. ISBN 978-85-7300-391-8.
- Ferreira, G., Hopkins, M., 2004. Manual de identificação botânica e anatômica angelim. Embrapa Amazônia Oriental, Belém, ISBN 8587690337
- Fichtler, E., Clark, D., Worbes, M., 2003. Age and long-term growth of trees in an old-growth tropical rain forest, based on analyses of tree rings and 14C. Biotropica 35, 306–317. http://www.istor.org/stable/30043047.
- Flora do Brasil 2020, 2021. Flora do Brasil 2020. In: Jardim Botânico do Rio de Janeiro. http://floradobrasil.jbrj.gov.br/. (Accessed 9 August 2021).
- Fritts, H.C., 1976. Tree Rings and Climate. Academic Press, London, pp. 1–567.
- Gaudinski, J.B., Torn, M.S., Riley, W.J., Swanston, C., Trumbore, S.E., Joslin, J.D., Majdi, H., Dawson, T.E., Hanson, P.J., 2009. Use of stored carbon reserves in growth of temperate tree roots and leaf buds: analyses using radiocarbon measurements and modeling. Global Change Biol. 15 (4), 992–1014. https://doi.org/10.1111/j.1365-2486.2008.01736.x.
- Gomes, V.H.F., Vieira, I.C.G., Salomão, R.P., et al., 2019. Amazonian tree species threatened by deforestation and climate change. Nat. Clim. Change 9, 547–553. https://doi.org/10.1038/s41558-019-0500-2.
- Granato-Souza, D., Stahle, D.W., Barbosa, A.C., Feng, S., Torbenson, M.C., de Assis Pereira, G., Schéongart, J., Barbosa, J.P., Griffin, D., 2018. Tree rings and rainfall in the equatorial Amazon. Clim. Dynam. 1–13. https://doi.org/10.1007/s00382-018-4227-y
- Granato-Souza, D., Stahle, D.W., Torbenson, M.C.A., Howard, I.M., Barbosa, A.C., Feng, S., Schongart, J., 2020. Multi-decadal changes in wet season precipitation totals over the eastern Amazon. Geophys. Res. Lett. https://doi.org/10.1029/2020GL087478.
- Guimarães, L.A.D.O.P., Dias, L.E., Rocha, G.C., Assis, I.R.D., Fernandes, R.B.A., 2018. Physical quality of bauxite tailing after a decade of environmental recovery. Rev. Cienc. Agron. 49, 192–200.
- Hadad, M.A., Santos, G.M., Juñent, F.A.R., Grainger, C.S., 2015. Annual nature of the growth rings of Araucaria araucana confirmed by radiocarbon analysis. Quat. Geochronol. 30, 42–47. https://doi.org/10.1016/j.quageo.2015.05.002.
- Haines, H.A., Olley, J.M., English, N., Hua, Q., 2018. Anomalous ring identification in two Australian subtropical Araucariaceae species permits annual ring dating and growth-climate relationship development. Dendrochronologia 49, 16–28. https:// doi.org/10.1016/i.dendro.2018.02.008.
- Herrera-Ramirez, D., Andreu-Hayles, L., Del Valle, J.I., Santos, G., Gonzalez, P.L.M., 2017. Nonannual tree rings in a climate sensitive Prioria copaifera chronology in the Atrato River, Colombia. Ecol. Evol. 7, 6334–6345. https://doi.org/10.1002/ ecol. 2005
- Hogg, A., Heaton, T.J., Hua, Q., Palmer, J.G., Turney, C.S.M., Southon, J., Bayliss, A., Blackwell, P.G., Boswijk, G., Bronk Ramsey, C., Pearson, C., Petchey, F., Reimer, P., Reimer, R., Wacker, L., 2020. SHCal20 Southern Hemisphere calibration, 0-55,000 years cal BP. Radiocarbon 62 (4), 759–778. https://doi.org/10.1017/RDC.2020.59.
- Hoch, G., 2015. Carbon reserves as indicators for carbon limitation in trees. In: Progress in Botany. Springer, Cham, pp. 321–346. https://doi.org/10.1007/978-3-319-08807-5 13.

- Hua, Q., Barbetti, M., Zoppi, U., Chapman, D.M., Thomson, B., 2003. Bomb radiocarbon in tree rings from northern New South Wales, Australia: implications for dendrochronology, atmospheric transport, and air-sea exchange of CO2. Radiocarbon 45, 431–447. https://doi.org/10.1017/S0033822200032793.
- Hua, Q., Barbetti, M., Levchenko, V.A., D'Arrigo, R.D., Buckley, B.M., Smith, A.M., 2012. Monsoonal influences on southern hemisphere <sup>14</sup>CO<sub>2</sub>. Geophys. Res. Lett. 39, L19806 https://doi.org/10.1029/2012GL052971.
- Hua, Q., Barbetti, M., Rakowski, A.Z., 2013. Atmospheric radiocarbon for the period 1950–2010. Radiocarbon 55 (4), 2059–2072. https://doi.org/10.2458/azu\_js\_rc. v55i2.16177.
- Hua, Q., Turnbull, J.C., Santos, G.M., Rakowski, A.Z., Ancapichún, S., De Pol-Holz, R., Hammer, S., Lehman, S.J., Levin, I., Miller, J.B., Palmer, J.G., 2021. Atmospheric radiocarbon for the period 1950–2019. Radiocarbon 1–23. https://doi.org/10.1017/ RDC.2021.95.
- Hughes, M.K., Swetnam, ThomasW., Diaz, H.F., 2011. Dendroclimatology. Springer Netherlands, Dordrecht.
- Igogo, T., Awuah-Offei, K., Newman, A., Lowder, T., Engel-Cox, J., 2021. Integrating renewable energy into mining operations: opportunities, challenges, and enabling approaches. Appl. Energy 300, 117375.
- Kalnay, E., Kanamitsu, M., Kistler, R., Collins, W., Deaven, D., Gandin, L., et al., 1996. The NCEP/NCAR 40-year reanalysis Project. Bull. Am. Meteorol. Soc. 77, 437–471. https://doi.org/10.1175/1520-0477(1996)077
- Keel, S.G, Siegwolf, R.T., Körner, C., 2006. Canopy CO2 enrichment permits tracing the fate of recently assimilated carbon in a mature deciduous forest. New Phytol. 172 (2), 319–329.
- Levin, I., Kromer, B., Schmidt, M., Sartorius, H., 2003. A novel approach for independent budgeting of fossil fuel CO<sub>2</sub> over Europe by <sup>14</sup>CO<sub>2</sub> observation. Geophys. Res. Lett. 30 (23), 2194. https://doi.org/10.1029/2003GL018477.
- Lin, D.S.C., Caramaschi, P.É., 2005. Responses of the fish community to the flood pulse and siltation in a floodplain lake of the Trombetas River, Brazil. Hydrobiologia 545 (1), 75–91.
- Linares, R., Santos, H.C., Brandes, A.F.N., et al., 2017. Exploring the 14C bomb peak with tree rings of tropical species from the Amazon Forest. Radiocarbon 59, 303–313.
- Mainieri, C., Chimelo, J.P., 1989. Ficha de características das madeiras brasileiras. Instituto de Pesquisas Tecnológicas do Estado de São Paulo, São Paulo, ISBN 8509000468, p. 418.
- Martínez-Vilalta, J., Sala, A., Asensio, D., Galiano, L., Hoch, G., Palacio, S., Piper, F.I., Lloret, F., 2016. Dynamics of non-structural carbohydrates in terrestrial plants: a global synthesis. Ecol. Monogr. 86, 495–516. https://doi.org/10.1002/ecm.1231.
- Mason, M., 1997. A look behind trend data in industrialization: the role of transnational corporations and environmental impacts. Global Environ. Change 7 (2), 113–127.
- Maxwell, R.S., Larsson, L.A., 2021. Measuring tree-ring widths using the CooRecorder software application. Dendrochronologia 67. https://doi.org/10.1016/J. DENDRO 2021.125841.
- Michot, V., Vila, D., Arvor, D., Corpetti, T., Ronchail, J., Funatsu, B.M., Dubreuil, V., 2018. Performance of TRMM TMPA 3B42 V7 in replicating daily rainfall and regional rainfall regimes in the Amazon basin (1998–2013). Remote Sens. 10 (12), 1879. https://doi.org/10.3390/rs10121879.
- Mildner, M., Bader, M.F., Leuzinger, S., Siegwolf, R.W., K€orner, C., 2014. Long-term 13C labeling provides evidence for temporal and spatial carbon allocation patterns in mature Picea abies. Oecologia 175, 747–762. https://doi.org/10.1007/s00442-
- Morales, M.S., Cook, E.R., Barichivich, J., Christie, D.A., Villalba, R., LeQuesne, C., Srur, A.M., Ferrero, M.E., González-Reyes, A., Couvreux, F., Matovsky, V., Aravena, J.C., Lara, A., Mundo, I.A., Rojas, F., Prieto, M.R., Smerdon, J.E., Bianchi, L.O., Masiokas, M.H., Urrutia, R., Rodriguez-Catón, M., Muñoz, A.A., Rojas-Badilla, M., Alvarez, C., Lopez, L., Luckman, B., Lister, D., Harris, I., Jones, P.D., Williams, A.P., Velazquez, G., Aliste, D., Aguilera-Betti, I., Marcotti, E., Flores, F., Muñoz, T., Cuq, E., Boninsegna, J.A., 2020. Six hundred years of South American tree rings reveal an increase in severe hydroclimatic events since mid-20th century. In: Proceedings of the National Academy of Sciences. https://doi.org/10.1073/pnas.2002411117.
- Morris, H., Jansen, S., 2016. Secondary xylem parenchyma from classical terminology to functional traits. IAWA J. 37, 1–15. https://doi.org/10.1163/22941932-20160117
- Morris, H., Plavcová, L., Cvecko, P., et al., 2016. A global analysis of parenchyma tissue fractions in secondary xylem of seed plants. New Phytol. 209, 1553–1565. https:// doi.org/10.1111/nph.13737.
- Parrotta, J.A., Knowles, O.H., 2001. Restoring tropical forests on lands mined for bauxite: examples from the Brazilian Amazon. Ecol. Eng. 17 (2–3), 219–239.
- Plavcová, L., Jansen, S., 2015. The role of xylem parenchyma in the storage and utilization of nonstructural carbohydrates. In: Hacke, U. (Ed.), Functional and Ecological Xylem Anatomy. Springer International, Cham, Switzerland, pp. 209–234. https://doi.org/10.1007/978-3-319-15783-2\_8.
- Plavcová, L., Hoch, G., Morris, H., Ghiasi, S., Jansen, S., 2016. The amount of parenchyma and living fibers affects storage of nonstructural carbohydrates in young stems and roots of temperate trees. Am. J. Bot. 103, 603–612. https://doi.org/ 10.3732/ajb.1500489.
- Quarta, G., Rizzo, G.A., D'elia, M., Calcagnile, L., 2007. Spatial and temporal reconstruction of the dispersion of anthropogenic fossil CO2 by 14C AMS measurements of plant material. Nuclear Instruments and Methods in Physics Research Section B: Beam Interactions with Materials and Atoms 259 (1), 421–425. https://doi.org/10.1016/j.nimb.2007.02.006.
- Randerson, J.T., Enting, I.G., Schuur, E.A.G, Caldeira, K., Fung, I.Y., 2002. Seasonal and latitudinal variability of troposphere Δ14CO2: Post bomb contributions from fossil

- fuels, oceans, the stratosphere, and the terrestrial biosphere. Global Biogeochem. Cycles 16 (4), 1112. https://doi.org/10.1029/2002GB001876.
- Reimer, P.J., Austin, W.E., Bard, E., Bayliss, A., Blackwell, P.G., Ramsey, C.B., Butzin, M., Cheng, H., Edwards, R.L., Friedrich, M., Grootes, P.M., 2020. The IntCal20 Northern Hemisphere radiocarbon age calibration curve (0–55 cal kBP). Radiocarbon 62 (4), 725–757. https://doi.org/10.1017/RDC.2020.41.
- Richardson, A.D., Carbone, M.S., Keenan, T.F., Czimczik, C.I., Hollinger, D.Y., Murakami, P., Schaberg, P.G., Xu, X.M., 2013. Seasonal dynamics and age of stemwood nonstructural carbohydrates in temperate forest trees. New Phytol. 197, 850–861. https://doi.org/10.1111/nph.12042.
- Richardson, A.D., Carbone, M.S., Huggett, B.A., Furze, M.E., Czimczik, C.I., Walker, J.C., Xu, X., Schaberg, P.G., Murakami, P., 2015. Distribution and mixing of old and new nonstructural carbon in two temperate trees. New Phytol. 206, 590–597. https://doi. org/10.1111/nph.13273.
- Rodgers, K.B., Mikaloff-Fletcher, S.E., Bianchi, D., Beaulieu, C., Galbraith, E.D., Gnanadesikan, A., Hogg, A.G., Iudicone, D., Lintner, B.R., Naegler, T., Reimer, P.J., Sarmiento, J.L., Slater, R.D., 2011. Interhemispheric gradient of atmospheric radiocarbon reveals natural variability of Southern Ocean winds. Clim. Past 7, 1123–1138. https://doi.org/10.5194/cp-7-1123-2011.
- Santos, G.M., Linares, R., Lisi, C.S., Tomazello Filho, M., 2015. Annual growth rings in a sample of Paraná pine (Araucaria angustifolia): toward improving the 14C calibration curve for the Southern Hemisphere. Quat. Geochronol. 25, 96–103. https://doi.org/10.1016/j.quageo.2014.10.004.
- Santos, G.M., Xu, X., 2017. Bag of tricks: a set of techniques and other resources to help 14C laboratory setup, sample processing, and beyond. Radiocarbon 59 (3), 785–801. https://doi.org/10.1017/RDC.2016.43.
- Santos, G.M., Granato-Souza, D., Barbosa, A.C., Oelkers, R., Andreu-Hayles, L., 2020. Radiocarbon analysis confirms annual periodicity in Cedrela odorata tree rings from the equatorial Amazon. Quat. Geochronol. 58, 101079 https://doi.org/10.1016/j. quageo.2020.101079.
- Santos, G.M., Rodriguez, D.R.O., Barreto, N.D.O., Assis-Pereira, G., Barbosa, A.C., Roig, F.A., Tomazello-Filho, M., 2021. Growth assessment of native tree species from the Southwestern Brazilian Amazonia by post-AD 1950 14C analysis: implications for tropical dendroclimatology studies and atmospheric 14C reconstructions. Forests 12 (9), 1177. https://doi.org/10.3390/F12091177.
- Scarchilli, C., Frezzotti, M., Rutti, P., 2011. Snow precipitation at four ice core sites in East Antarctica: provenance seasonality a blocking factors. Climate Dyn. 37, 2107–2125. https://doi.org/10.1007/s00382-010-0946-4.
- Schlosser, E., Oeter, H., Mason-Delmonte, V., Reijmer, C., 2008. Atmospheric influence on the deuterium excess signal in polar firn: implications for ice-core interpretation. J. Glaciol. 54, 117–124. https://doi.org/10.3189/002214308784408991.
- Schulman, E., 1956. Dendroclimatic Changes in Semiarid America. University of Arizona Press. Tucson.
- Sinclair, K., Bertler, N., Trompetter, W., Baisden, W., 2013. Seasonality of airmass pathways to coastal Antarctica: ramifications for interpreting high-resolution ice core records. J. Clim. 26 (6), 2065–2076. https://doi.org/10.1175/JCLI-D-12-00167.1.
- Slotta, F., Wacker, L., Riedel, F., Heußner, K.U., Hartmann, K., Helle, G., 2021. High-resolution 14 C bomb peak dating and climate response analyses of subseasonal stable isotope signals in wood of the African baobab–a case study from Oman. Biogeosciences 18 (12), 3539–3564. https://doi.org/10.5194/bg-18-3539-2021.
- Stein, A., Draxler, R., Rolph, G., Stunder, B., Cohen, M., Ngan, F., 2015. NOAA's HYSPLIT atmospheric transport and dispersion modeling system. Bull. Am. Meteorol. Soc. 96, 2059–2077. https://doi.org/10.1175/BAMS-D-14-00110.1.
- Stuiver, M., Polach, H., 1977. Discussion: reporting of <sup>14</sup>C data. Radiocarbon 19 (3), 355–363. https://doi.org/10.1017/S0033822200003672.
- Sonter, L.J., Herrera, D., Barrett, D.J., Galford, G.L., Moran, C.J., Soares-Filho, B.S., 2017. Mining drives extensive deforestation in the Brazilian Amazon. Nat. Commun. 8 (1), 1–7.
- Speer, J.H., 2010. Fundamentals of Tree-Ring Research. The University of Arizona Press, Arizona.
- Spicer, R., 2014. Symplasmic networks in secondary vascular tissues: parenchyma distribution and activity supporting long-distance transport. J. Exp. Bot. 65, 1829–1848. https://doi.org/10.1093/jxb/ert459.
- Tans, P., 2022. Reminiscing on the use and abuse of 14C and 13C in atmospheric CO2. Radiocarbon 1–14. https://doi.org/10.1017/RDC.2022.7.
- Trumbore, S., Czimczik, C.İ., Sierra, C.A., Muhr, J., Xu, X., 2015. Non-structural carbon dynamics and allocation relate to growth rate and leaf habit in California oaks. Tree Physiol. 35, 1206–1222. https://doi.org/10.1093/treephys/tpv097.
- Turney, C.S.M., Palmer, J., Maslin, M.A., et al., 2018. Global peak in atmospheric radiocarbon provides a potential definition for the onset of the anthropocene epoch in 1965. Sci. Rep. 8, 1–10. https://doi.org/10.1038/s41598-018-20970-5.
- Vásquez, M., Lara, W., del Valle, J.I., Seirra, C.A., 2022. Reconstructing past fossil-fuel CO2 concentrations using tree rings and radiocarbon in the urban area of Medellín, Colombia. Environ. Res. Lett. https://doi.org/10.1088/1748-9326/ac63d4.
- Vuille, M., Burns, S., Taylor, B., Cruz, F., Bird, B., Abbott, M., et al., 2012. A review of the South American monsoon history as recorded in stable isotopic proxies over the past two millennia. Clim. Past 8, 1309–1321. https://doi.org/10.5194/cp-8-1309-2012.
- Wang, W.W., Pataki, D.E., 2010. Spatial patterns of plant isotope tracers in the Los Angeles urban region. Landsc. Ecol. 25, 35–52.
- Wheeler, E.A., Baas, P., Rodgers, S., 2007. Variations in dicot wood anatomy: a global analysis based on the Insidewood database. IAWA J. 28, 229–258. https://doi.org/ 10.1163/22941932-90001638.
- Wils, T.H., Robertson, I., Eshetu, Z., Sass-Klaassen, U.G., Koprowski, M., 2009.Periodicity of growth rings in Juniperus procera from Ethiopia inferred from

crossdating and radiocarbon dating. Dendrochronologia 27, 45–58. https://doi.org/10.1016/j.dendro.2008.08.002.

Worbes, M., Junk, W., 1989. Dating tropical trees by means of 14C from bomb tests. Ecology 70, 503–507. https://doi.org/10.2307/1937554.

Xing, H., Stuart, C., Spence, S., Chen, H., 2021. Alternative fuel options for low carbon maritime transportation: pathways to 2050. J. Clean. Prod. 297, 126651.